[9.9]

The Sintering of Crystalline Oxides, II. Densification and Microstructure Development in UO$_2$

B. Francois

Departement de Metallurgie, Service de Chimie des Solides, Section des Combustibles Ceramiques

&

W. D. Kingery

Ceramics Department, Massachusetts Institute of Technology, Cambridge, Massachusetts

ABSTRACT

A study of the microstructure changes and density in UO$_2$ sintered with rapid heating in hydrogen shows that it is possible to obtain structures with all the residual porosity located at junctions between grains. When this occurs densification practically stops and the type of microstructure and the density remain stable over a wide range of time and temperature.

A small concentration of carbon (of the order of 10 ppm) reacting to form CO at a critical point during sintering is believed to be responsible for this behavior. This interpretation is supported by the geometry of the pores and by direct analysis of the carbon extracted as CO after sintering.

I   INTRODUCTION

The microstructure of UO$_2$ sintered in hydrogen under normal industrial conditions generally resembles that shown in Fig. 1a. The residual porosity consists partly of relatively large pores situated on grain boundaries or collected in groups and partly of more numerous smaller pores located within the grains. We shall refer to this type of porosity as 'intergranular'.

In contrast, during laboratory sintering studies we have observed microstructures such as shown in Fig. 1b, wherein the residual porosity is situated solely on grain boundaries, usually at grain boundary intersections [1]. With this type of structure the density and general appearance of the microstructure

467

(a)

(b)

Fig. 1. Typical microstructures illustrating: (a) intergranular porosity (400×); (b) intergranular porosity (400×).

remain stable over a wide domain of time and temperature. We shall refer to this type of porosity as 'intergranular'.

Two factors have been previously reported to favor the appearance of this special microstructure: increasing the specific surface area of the UO_2 powder used, and increasing the rate of temperature rise during sintering [2]. A third factor which we have found to be equally important is to increase the green density of the pressed compact. Figure 2 shows typical results obtained for density and microstructure as a function of sintering temperature and of green density. Similar results have been reported elsewhere [3].

In the present research, we have studied the factors responsible for this special type of densification and microstructure development.

II EXPERIMENTAL METHODS

1 Materials

The UO_2 powder used was prepared by decomposing ammonium diuranate to form UO_3 (surface area $20 \, m^3/gm$) followed by reduction at 380–400°C to give
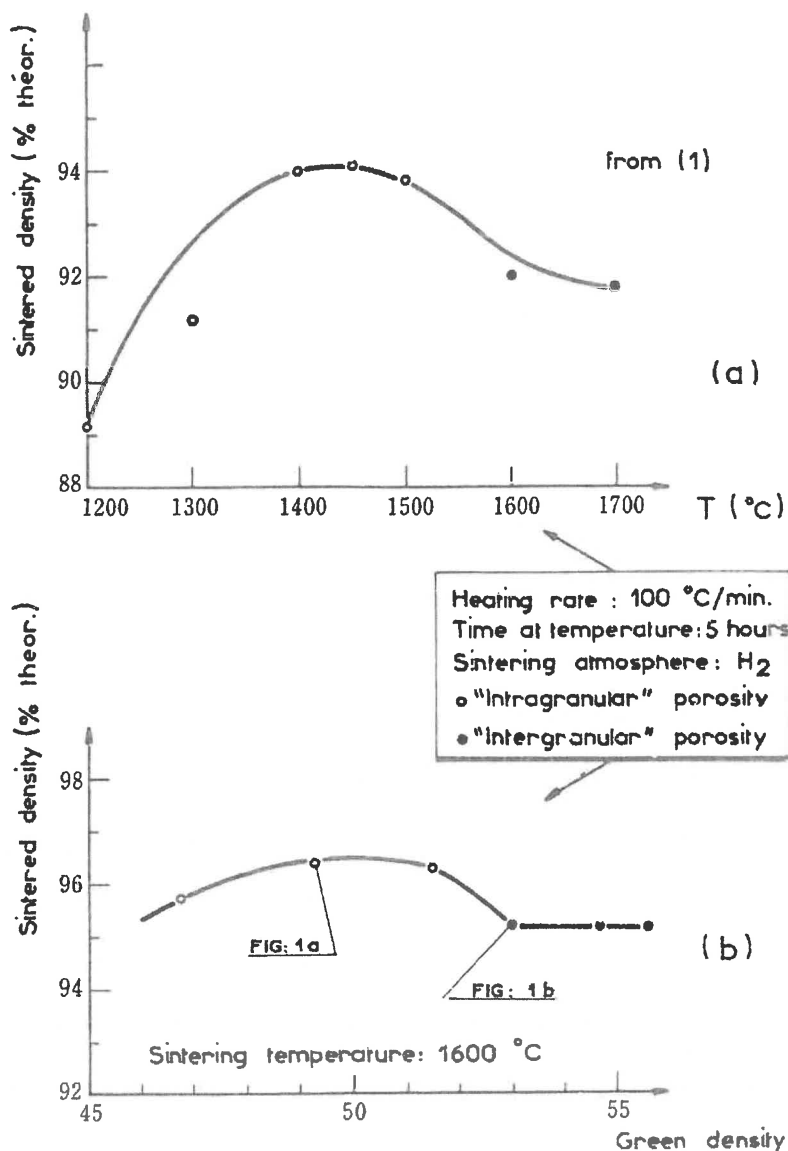
Fig. 2. Effect of (a) firing temperature (b) green density on final density and type of microstructure.

UO_2 having a surface area $\geqslant 10 \ m^2/gm$. After reduction the powder reoxidized on standing at room temperature to give a starting material having a composition near $UO_{2,20}$; its physicochemical characteristics are given in Table 1.

2 Powder Compaction

The powder was homogenized by dry-screening to give aggregates $< 160 \ \mu$, then pressed without any additions into cylinders 10 mm in diameter by 10 mm

Table 1

Physico-Chemical Characteristics of Powder Used

Specific surface area B.E.T. (m^2/g)	Average particle diameter (μ) Blaine	O/U ratio	Crystal structure (X-Ray)
12($\pm$1)	0.3_8	2.21	Cubic fluorite (UO_2)

Impurities Amounts (p.p.m./U)

Metals								Carbon (total)
Al	B	Cr	Cu	Fe	Mn	Ni	Si	
35	0.1	6	25	26	<5	5	55	215 $\pm$ 10

high. The die wall was lubricated with a light coating of stearic acid in ether (experience has shown that the small carbon contamination thus introduced is rapidly eliminated at a temperature near 400°C, and in any event affects only a thin surface layer of the samples).

The effect of pressure on green density is shown in Fig. 3. After preliminary tests, three pressures were selected for more detailed study:

A − 4.0 tons/cm^2 giving a green density of 49.3% theoretical
B − 5.5 tons/cm^2 giving a green density of 52.0% theoretical
C − 7.0 tons/cm^2 giving a green density of 54.9% theoretical

(Green densities were constant ± 0.2%; theoretical density is 10.97 gm/cc).

3 Sintering

Sintering was done in a continuous molybdenum resistance alumina tube laboratory furnace. Temperatures were checked with an optical pyrometer and controlled ± 3°C with a WRe 5%–WRe 26% thermocouple. The sintering atmosphere was hydrogen containing 2–3% water vapor. Several parallel experiments using a tungsten resistance furnace showed that similar results were obtained in an atmosphere of dry hydrogen (20 ppm H$_2$O).

The firing cycle consisted of:

(a) heating from room temperature to 900°C (where sintering begins [4], as indicated by a decreased surface area) at a rate of 16°C/minute, with two arrests of 30 minutes each at 320°C and 600°C, after which the composition was essentially stoichiometric (O/U < 2.01);

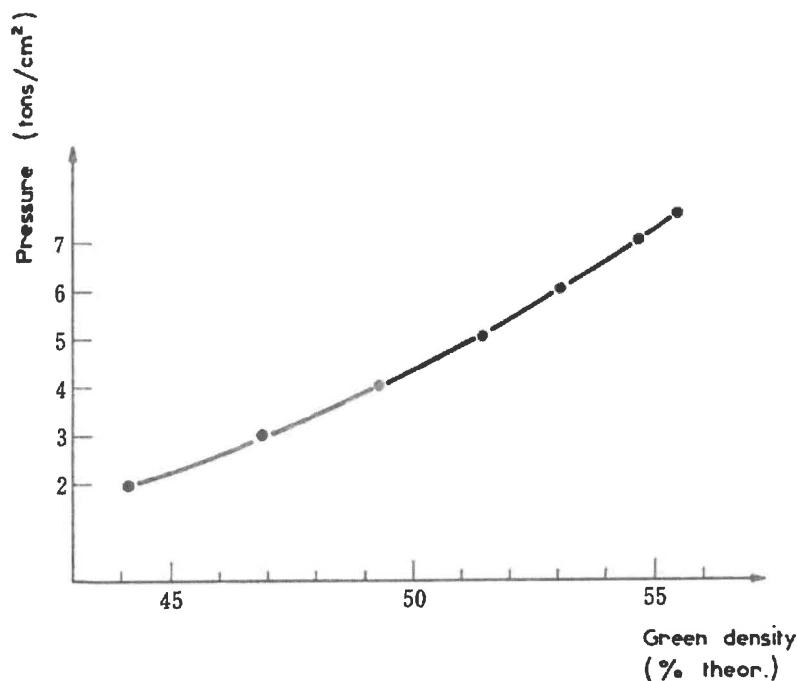(b) heating from 900°C to the sintering temperature at a rate of

Fig. 3. Effect of forming pressure on green density.

100°C/minute by manually pushing the samples through the temperature gradient in the furnace, and

(c) carrying out isothermal treatments at 1400, 1500, 1600, or 1700°C for periods ranging from 20 seconds to 300 minutes. (Temperature measurement shows that twenty seconds is approximately the time required for the center of the sample to reach the sintering temperature; during heating the surface is about 25°C hotter than the center).

4 Examination After Sintering

Density was measured by hydrostatic weighing in toluene introduced under vacuo during 20 minutes. Measurements of open porosity less than 0·5% are not considered significant.

Microscopic examinations were made of the center portion of a sample after mechanical polishing and etching with $H_2O_2 + H_2SO_4$ to reveal grain boundaries. Such etching does not measurably change the size or shape of pores. Grain size and pore size were determined by linear analysis.

III   RESULTS

In general, results given for 20 seconds should be accepted with some caution because of the difficulty in defining precisely that short time.
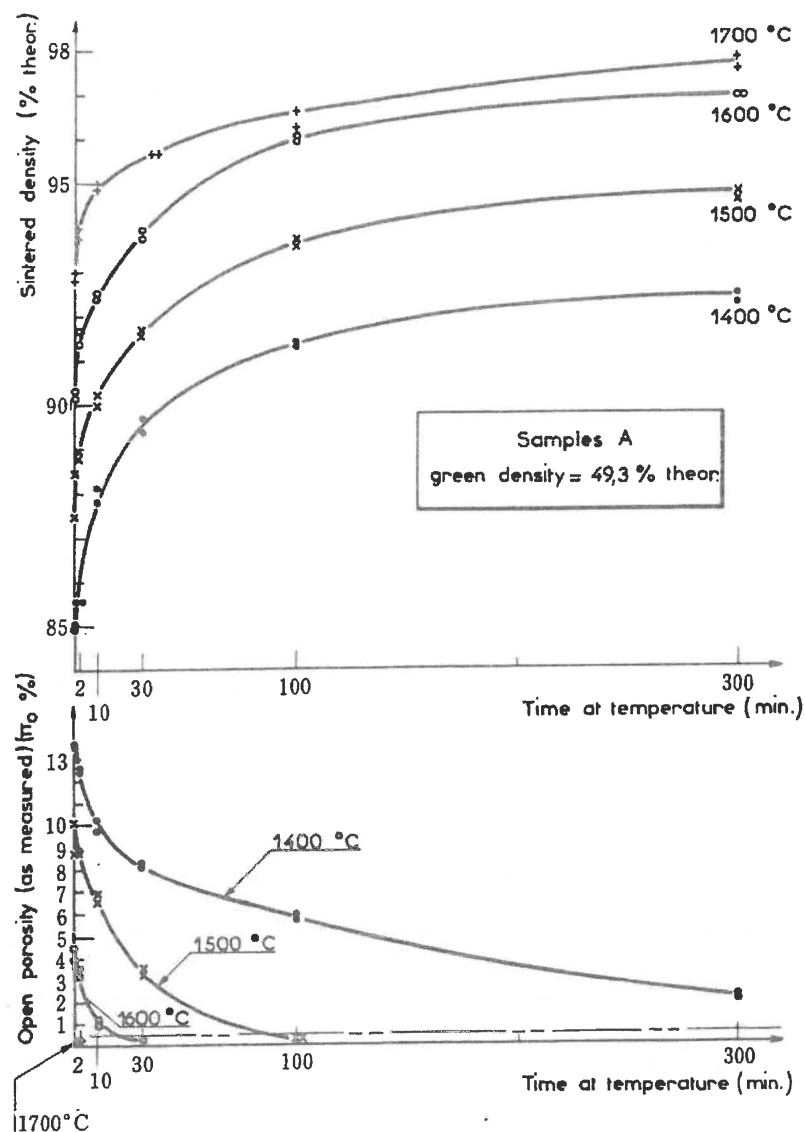
Fig. 4. Increase in density and decrease of open porosity of type 'A' samples (green density 49·3% of theoretical) with sintering time at different temperatures.

1 Densification

Values of density measured are shown in Fig. 4 for samples 'A' (green density = 49·3% of theoretical) and in Fig. 5 for samples 'C' (green density = 54·9% of theoretical). These figures also show the open porosity, found to be negligible when the density is greater than 93% of theoretical. With the sintering cycle used it should be noted that the larger part of the density change occurs during the few minutes while the temperature is still rising. Mean values found after 20 seconds at temperature are shown in Fig. 6. At
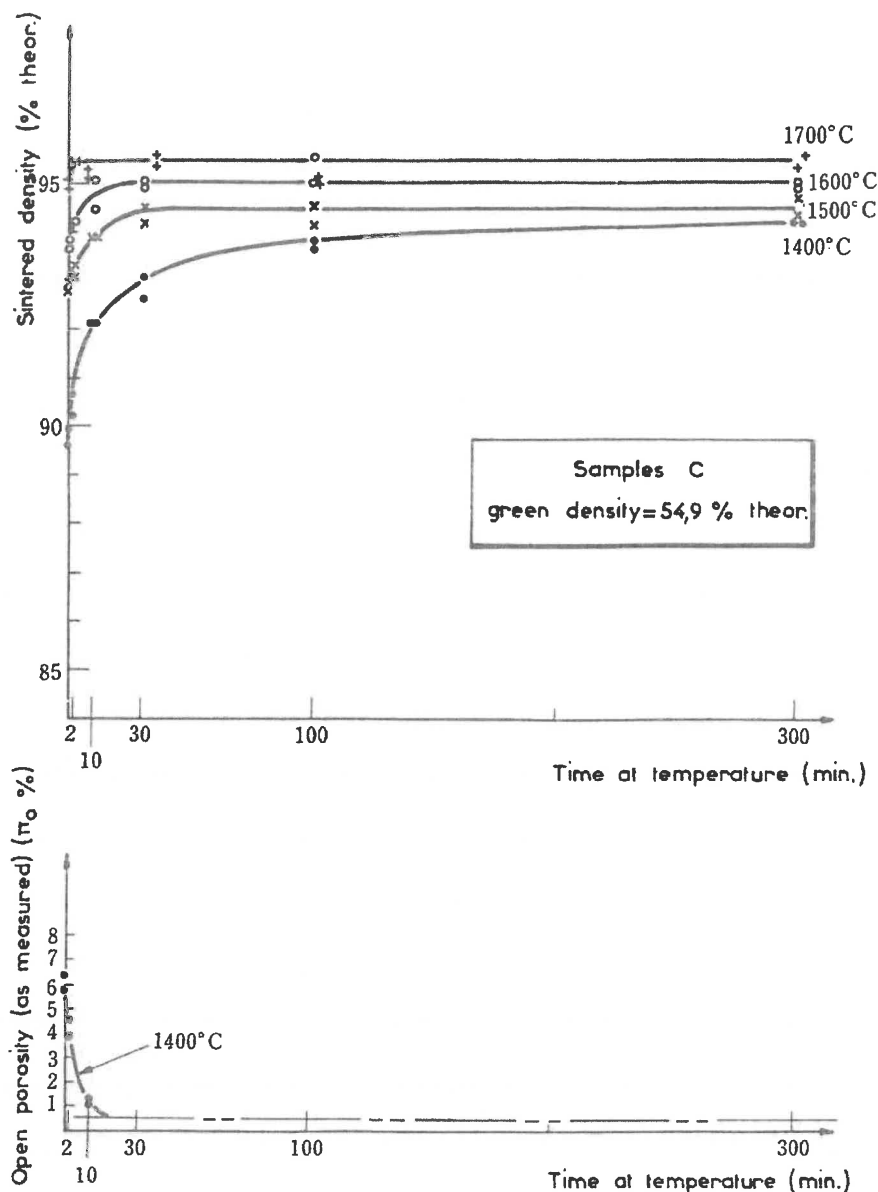
Fig. 5. Increase in density and decrease of open porosity of type 'C' samples (green density 54·9% of theoretical) with sintering time at different temperatures.

1400°C and 1500°C the difference in density found after 20 seconds is just equal to the difference in green density.

For samples 'A' (green density = 49·3% of theoretical) density increases with temperature and with time at temperature, as is generally found. The open porosity becomes negligible after the times shown in Table 2, and high final densities are reached after 300 minutes; i.e. 96·9% theoretical at 1600°C and 97·7% theoretical at 1700°C.
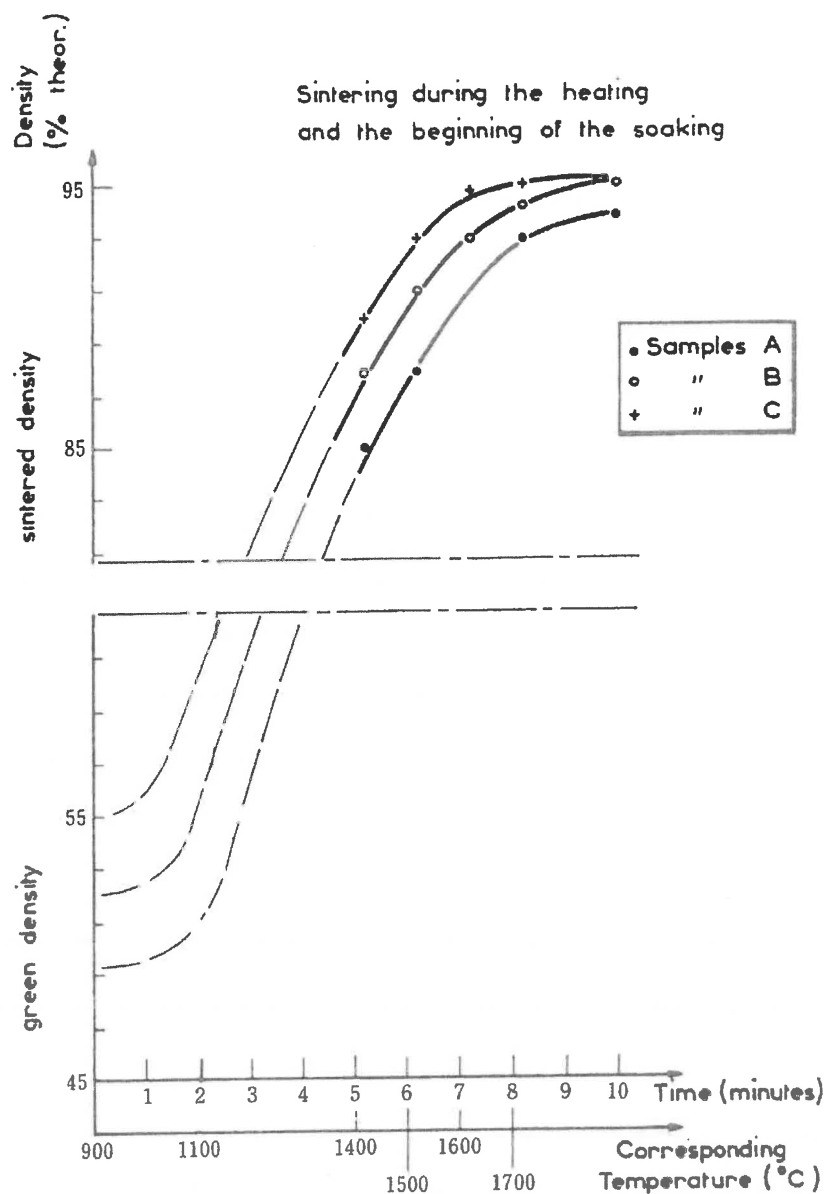
Fig. 6. Progress of sintering during heating shown for samples of different green density.

For samples 'C' (green density = 54·9% of theoretical) the increased density arising from the higher compaction pressure persists during the time of heating, and an advantage is maintained at 1400°C. However, the density reaches a limit of the order of 95% theoretical after 30 minutes at 1500°C, 10 minutes at 1600°C, and 2 minutes at 1700°C (see Fig. 5). As shown in Table 2 the open porosity very quickly becomes negligible.

Table 2
Time Required for Elimination of Open Porosity

Sample	Time required for elimination of open porosity (min)			
	1400°C	*1500°C*	*1600°C*	*1700°C*
A	>300	30–100	10–30	~0
B	100–300	10–30	~0	~0
C	10–30	~0	~0	~0

Samples 'B' (green density = 52·0% of theoretical) show intermediate behavior and only reach a clear density limit after 30 minutes at 1700°C.

2 Microstructure

2.1 *Samples (type 'A') with essentially intragranular porosity*
The micrographs of Fig. 7, a typical example, show that most of the pores remain inside the grains, corresponding to the usual structure reported for sintered UO_2.

The kinetics of grain growth are illustrated for 1600°C in Fig. 8. (At lower temperatures the small grain size makes meaningful measures difficult). Taking the initial grain size as zero as $t = 0$, grain growth follows the relation $D = kt^n$, with $n = 0·31$, closely approaching the theoretical value of $n = 0·33$ [5].

Table 3 gives some measured values of the ratio $1_p/1_g$ = mean pore diameter/mean grain diameter, of pores situated in grain boundaries, during grain growth of type 'A' samples. That ratio decreases with time at temperature; at the same time the density is increasing.

2.2 *Samples (type 'C') with intergranular porosity*
The microstructures of Fig. 9 for samples at 1600°C are typical of this type of porosity. (At the very edge of the samples there was a peripheral zone of smaller grains and intragranular porosity (see ref. 1) with behavior similar to samples 'A'. That zone results neither from fabrication conditions nor from thermal gradients. Rather it is caused by material exchange (either the introduction or loss of a contaminant) between the atmosphere and the sample surface.

Figure 9 shows that the localization of pores at grain boundaries occurs at very short times (20 seconds) at 1600°C and 1700°C. At 1500°C the grain size is small and observations are difficult but an intergranular microstructure is clearly established after 30 minutes, coincidental with the halting of further densification (Fig. 5). After 300 minutes at 1400°C, the same type of microstructure is observed. That is, at temperatures above 1500°C, an intergranular microstructure appears at short times, the order of one minute.
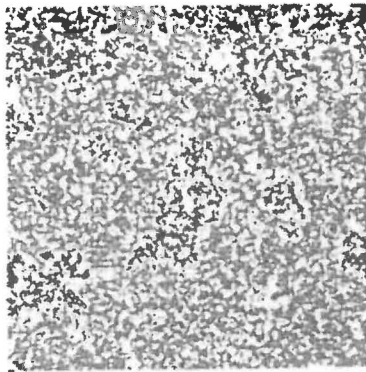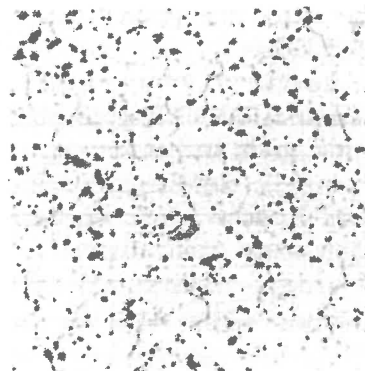
2 minutes
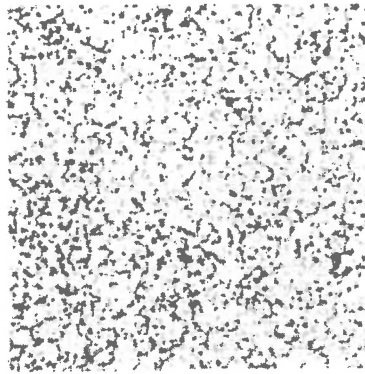
30 minutes
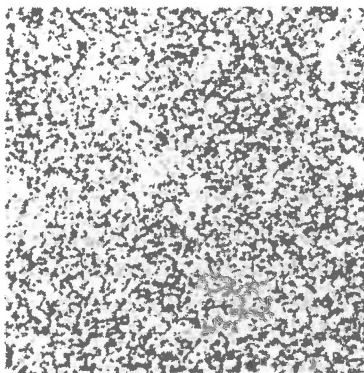
10 minutes

300 minutes

Fig. 7. Samples A, Sintering Temperature 1600°C. Microstructure development of type 'A' samples (green density 49·3% of theoretical) during sintering at 1600°C (800×).

While the appearance of this type of microstructure coincides with the effective blocking of further densification, both grain growth and pore growth (and a parallel decrease in their numbers per unit area) continued simultaneously at a constant density and in the absence of open porosity as shown in Fig. 10. Therefore, within the precision of experimental measurements, the ratio $1_p/1_g$ = pore size/grain size remains constant as shown in Table 3. Thus in this case, there clearly takes place a simultaneous displacement of pores and grain boundaries. The pores do not function as a second phase capable of completely blocking the movement of grain boundaries.
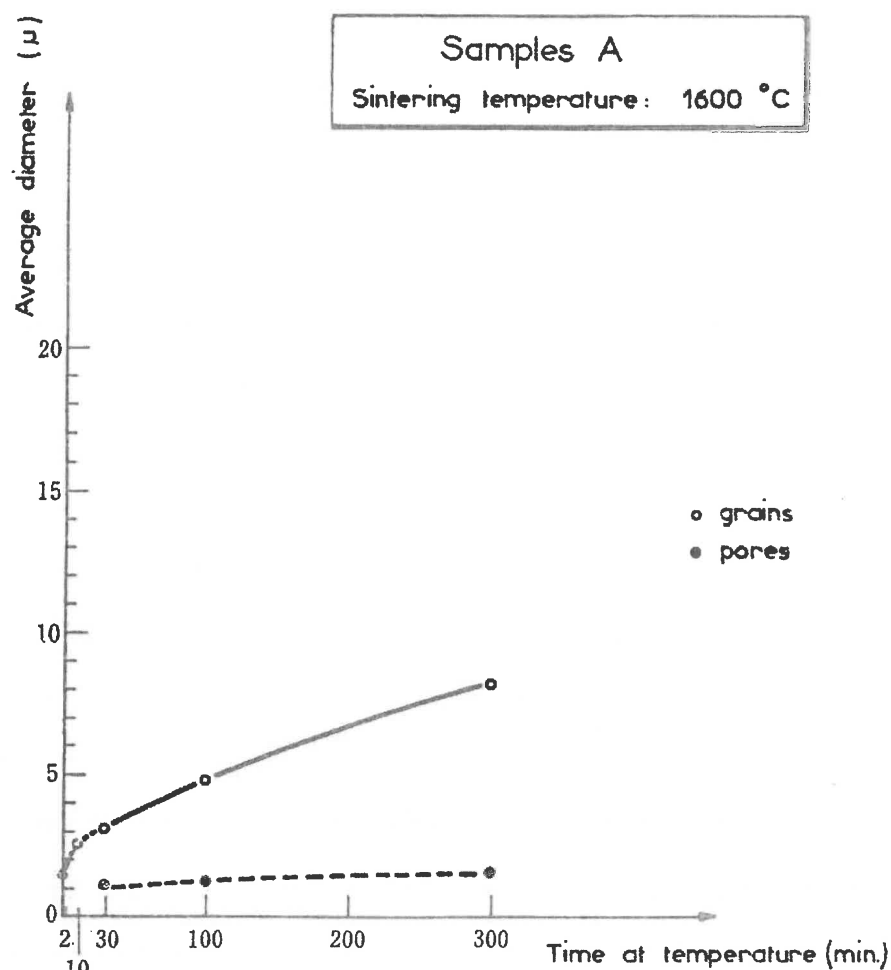
Fig. 8. Change in pore diameter and grain diameter of type 'A' samples during sintering at 1600°C.

Table 3
Ratio of Pore Diameter to Grain Diameter After Indicated Heat Treatments

Samples	Sintering temperature	Time of temperature					
		20 sec	2 min	10 min	30 min	100 min	300 min
A	1600°C				0.36^a	0.32^a	0.22^a
	1700°C			028^a	0.25^a	0.18^a	0.15^a
C	1400°C						0.28
	1500°C			0.30^a	0.30	0.26	0.24
	1600°C	0.29^a	0.29^a	0.28^a	0.22	0.25	0.26
	1700°C		0.26	0.23	0.19	0.21	0.17

Table shows $\dfrac{\text{Pore diameter}}{\text{Grain diameter}} = \dfrac{1p}{1g}$ against sintering time and temperature.

[a] Values corresponding to samples still shrinking, $\left(\text{therefore with decreasing } \dfrac{1p}{1g}\right)$.

B. Francois & W. D. Kingery

20 seconds

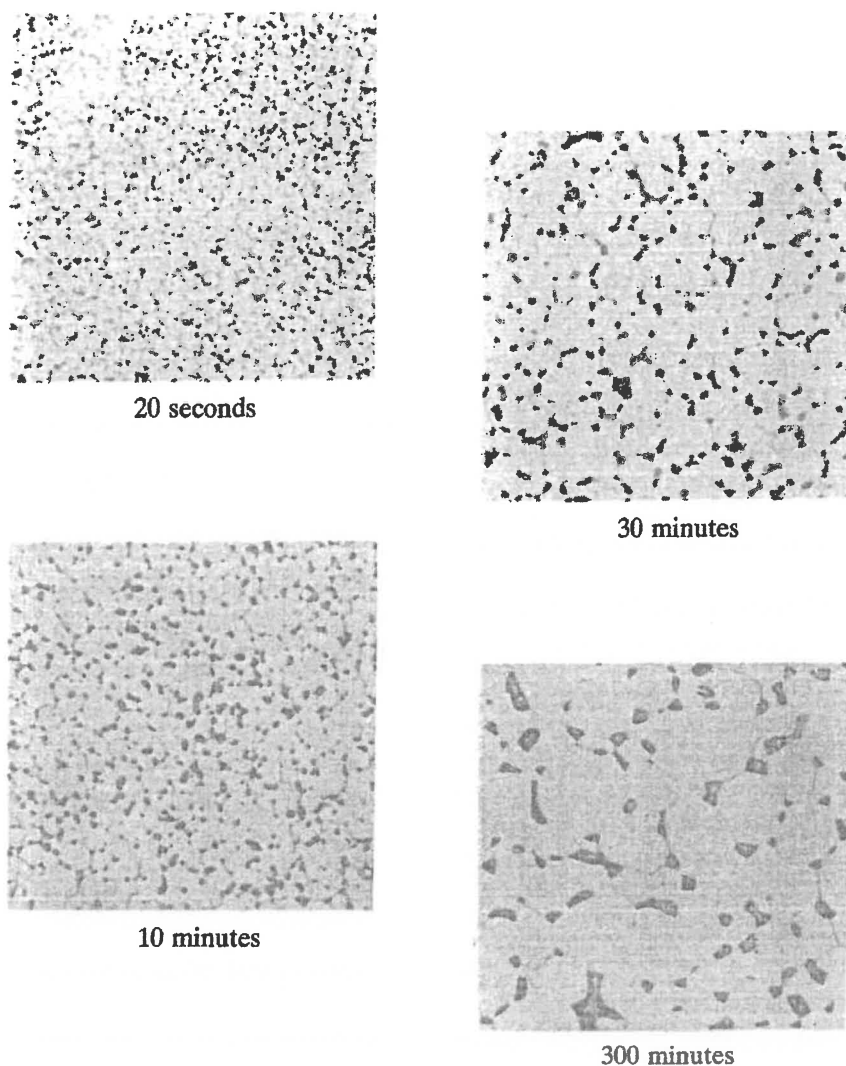**30 minutes**

10 minutes

300 minutes

Fig. 9. Samples C, Sintering Temperature: 1600°C. Microstructure development of type 'C' samples (green density 54·9% of theoretical) during sintering at 1600°C (400×).

With this type of microstructure the time dependence of both grain and pore growth is still of the form $D = kt^n$. Taking $D_0 = 0$ at $t = 0$, the values found for n are of the order of 0·3.

The grain size of these samples is distinctly greater than those of type 'A'.

No limit to grain size was observed here at times up to 300 minutes. However, in a previous study [1] it was noted with the same type of microstructure, but with a lower limiting density (92% theoretical compared with 95% theoretical here) that grain growth and pore growth appeared to stop
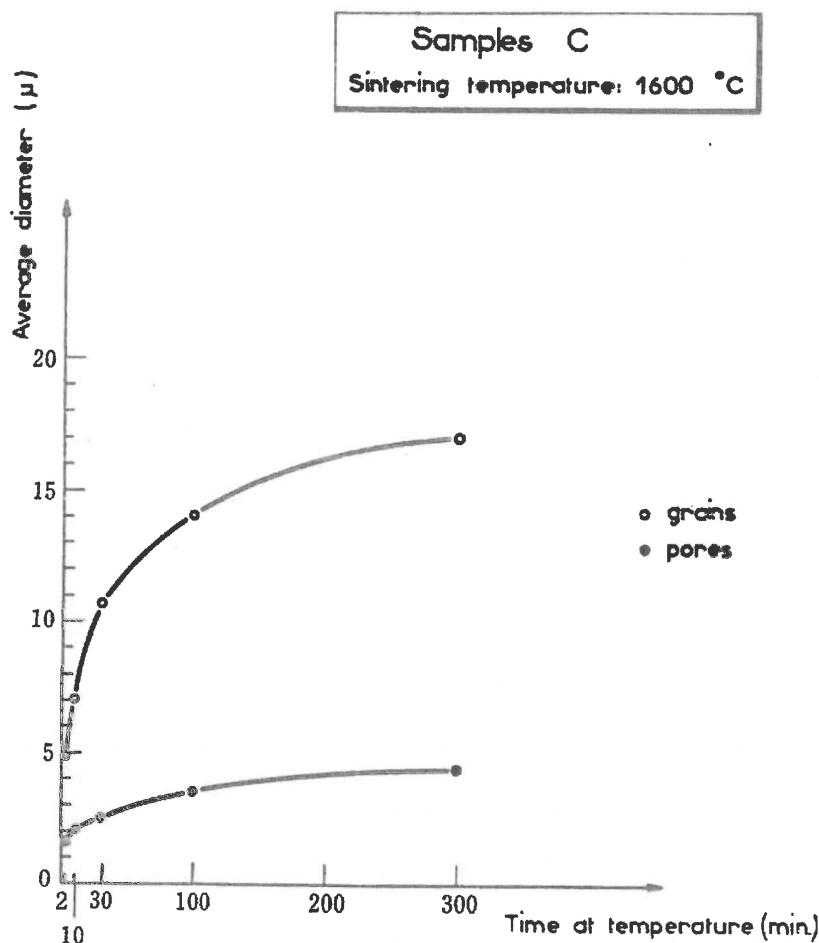
Fig. 10. Change in pore diameter and grain diameter of grains of type 'C' samples during sintering at 1600°C.

after 60 minutes at 1600°C. The density, grain size, pore size, and pore morphology remained unchanged even after 100 hours at 1600°C. An example of that stability after heat treating a sample sintered 300 minutes at 1600°C for 50 hours at 1800°C is shown in Table 4.

3 Morphology of the Intergranular Porosity

3.1 *Pore shape*

Figure 11 shows a typical histogram of the number of sides measured for pores intersected by a polished surface. Various experimental and analytical studies of the shape of plane sections through regular polyhedra [6–8] show that the most probable result for a cube is a polygon of four sides, (the most probable result in a slice through a tetrakaidecahedron is six, the most common result

B. *Francois & W. D. Kingery*

Table 4
Changes in Sintered Sample After Heating 50 Hours at 1800°C

Sample	Sintered density (% theor.)	Average pore diameter (μ)	Average grain diameter (μ)	$\dfrac{l_p}{l_g}$
Sintered 300 min at 1600°C	94·9	4·8	17·7	0·27
Same sample plus 50 hours at 1800°C	95·2	5·2	18·4	0·28

for polycrystalline ceramics). Thus Fig. 11 indicates that a large fraction of the pores are roughly cubic in form, that is, surrounded by six grains in space.

3.2 Dihedral angles

A typical histogram of pore-grain boundary dihedral angles is shown in Fig. 12. For that sample the most probable angle is 96°. Measurements on about twenty
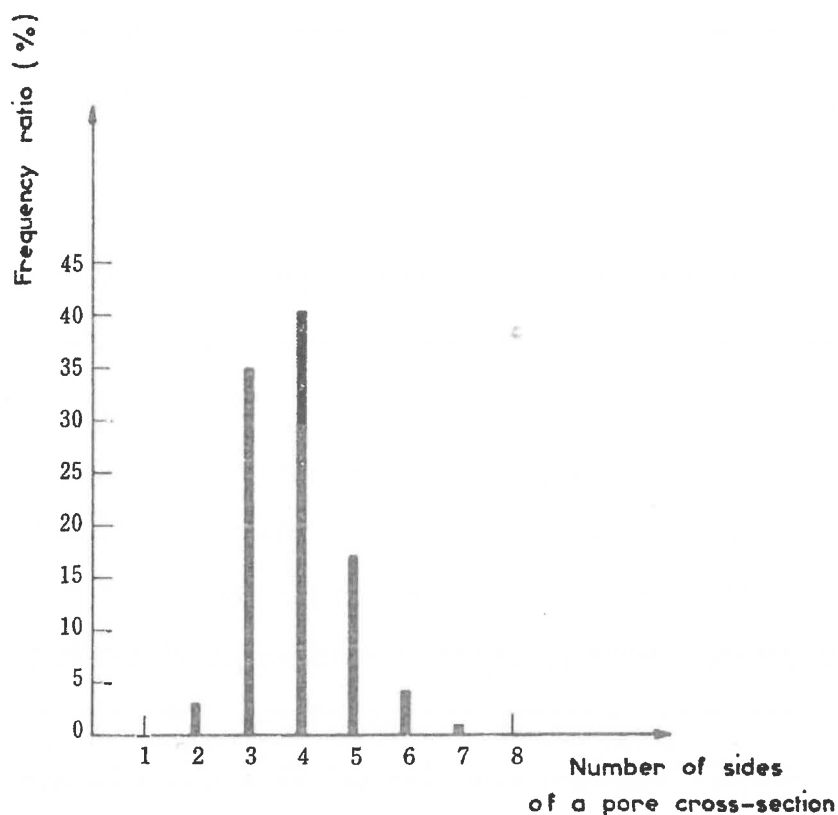

Fig. 11. Histogram showing the number of sides per pore in a plane section.
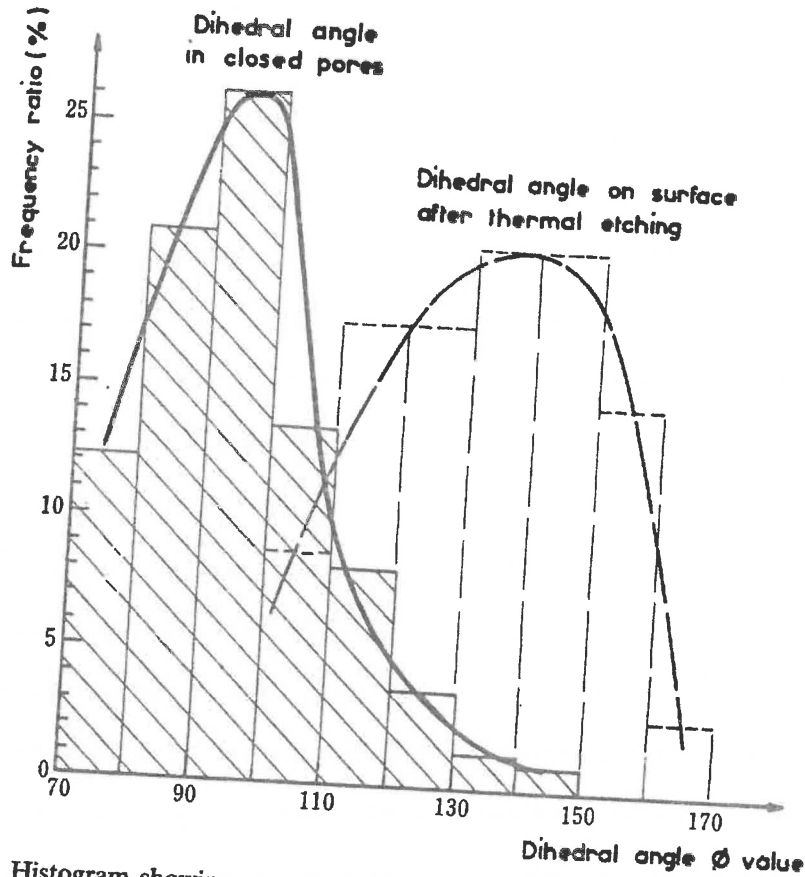
Fig. 12. Histogram showing measured values of dihedral angles at the interior and at the surface of a sample.

samples gave results varying between 87° and 97° with an overall average of 92°. It should be noted that these values are much smaller than those normally found: i.e., 152° for Al_2O_3 [9], 130° for $Al_2O_3 + 1/4\%$ MgO [10].

However, measurements of the dihedral angles at a surface of a sample heated at 1800°C for 50 hours give an angle near 140°, also shown in Fig. 12. This heat treatment gives considerable thermal etching of the grain boundaries at the surface and near-equilibrium values are to be expected.

IV   DISCUSSION

1   Pore Stability

The cube configuration of pores with an internal dihedral angle of 92° surrounded by six grains corresponds, as discussed by Kingery and Francois [11], to a condition of stability in which there is no tendency for pore shrinkage.

2   Difference Between Surface and Interior Dihedral Angles

The difference between the internal (92°) and surface (~140°) dihedral angles in samples with pores stable at grain intersections suggests at first that the surface energy of the pores in the interior is less than at an external surface. This might result from some chemisorption process, but it seems to be very improbable at these high temperatures. A second and more likely possibility is the existence of a gas phase trapped in the closed pores, which has been shown by us previously [11] to lead to a lower value of the dihedral angle. Analysis of gas extracted from the samples does indeed show the presence of carbon monoxide.

3   The Overall Course of Sintering

Our overall interpretation is that traces of carbon present in the samples react with the UO_2 during sintering to form carbon monoxide,

$$UO_2(s) + 3C(s) \rightleftharpoons UC(s) + 2CO(g)$$
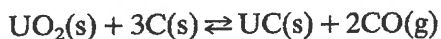
This reaction begins at 1200–1300°C and proceeds at a rate which increases with temperature. If the pores remain open during this process, the CO formed is able to escape and the residual porosity remains distributed at random resulting in the intragranular porosity found for samples 'A' where open porosity remains present at temperatures up to 1700°C and for usual industrial sintering processes carried out with a relatively slow rate of heating. When the CO formed is unable to escape, as for samples 'C', intergranular porosity and its accompanying microstructure result.

Several observations directly support this interpretation. First, the observed difference between the internal and surface dihedral angle. Second, our approximate calculation of the influence of gas pressure on the dihedral angle [11] is in accord with the amounts of carbon found to be present. By vacuum extraction we have measured the total carbon content of the samples after sintering. In this process all the carbon present is extracted as CO. Assuming that all the carbon found is also present as CO after sintering 300 minutes at 1600°C, and assuming that the residual porosity is completely closed and at the same pressure, the maximum possible CO pressure can be calculated with the results shown in Table 5. As illustrated in Fig. 13 there is a distinct difference between the maximum pressure estimated for samples with intragranular porosity (1–5 atm) and for those with intergranular porosity (10–50 atm). The latter values are of the same order of magnitude as had been estimated from the dihedral angles measured [11].

However, it is difficult to estimate with precision the actual kinetics of the two competing processes (CO formation and CO effusion) under the experimental conditions we have employed. There are several uncertainties, notably the quantity of reactive carbon present at the critical point in the process, the solubility of C and CO in UO_2, and the influence of the heating rate on the reaction process and its approach toward equilibrium.

As a further test of the influence of carbon contamination on densification,
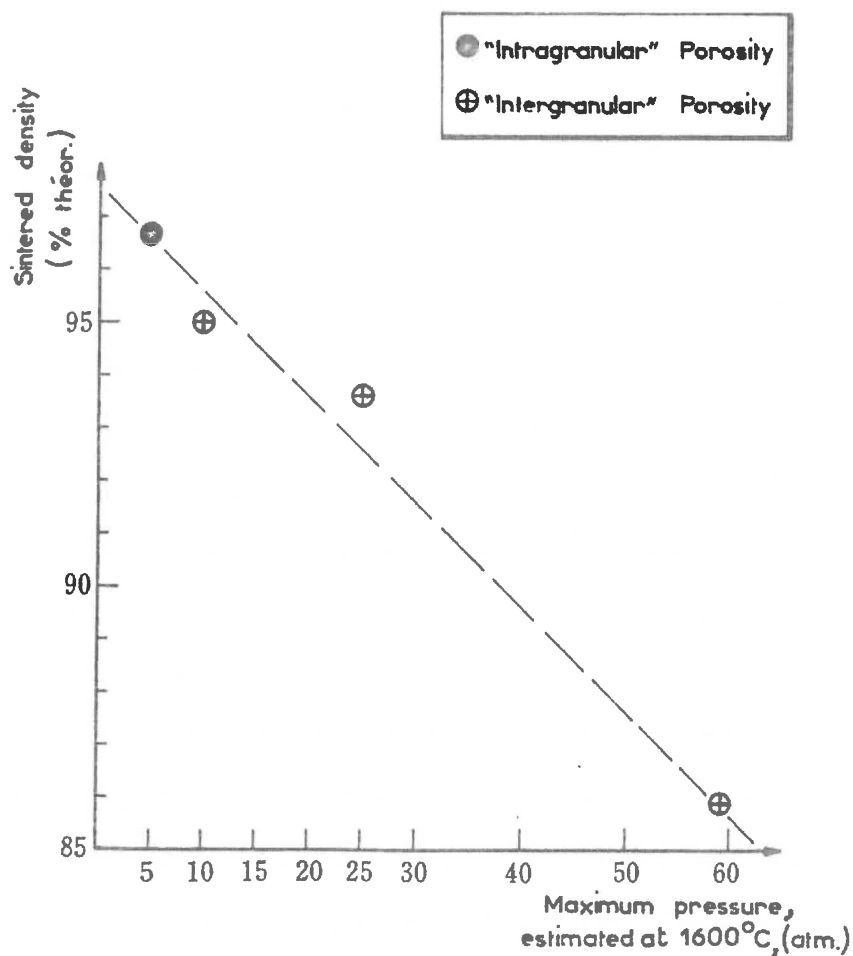
Fig. 13. Calculated values of maximum CO pressure correlated with the limiting density reached at 1600°C.

we prepared samples with additions of stearic acid introduced as a solution in ether. With such additions there was a distinct decrease in final density (85·9% theoretical as compared to 95·0% without addition) as shown in Table 5. If extensive carbon trapping is accomplished (by using a high green density) stearic acid additions cause swelling of the samples, and sometimes fissuration, indicating clearly that a gas pressure is developed and also that plastic deformation is possible.

4 Supporting Observations

The interpretation that CO formation is responsible for the microstructure and densification limit observed also serves to explain the influence of several parameters previously found to favor the appearance of intergranular porosity.

Increasing the surface area of the powder used is well known to increase the

Table 5

Measured CO Content (By Gas Extraction at 2000°C) and Estimated
Resulting Maximum Pressures

Sintered density (% theor.)	Type of porosity	CO (ppm/UO_2)	Maximum pressure estimated at 1600°C (atm.)
96·9	'Intragranular'	~3	(1 to) 5
96·4	"	~3	"
95	'Intergranular'	9	10
93·6	"	26	25
85·9[a]	"	180	~59

[a] With addition of stearic acid.

densification rate at intermediate temperatures and thus leads to the more rapid formation of closed pores, CO entrapment and intergranular porosity. In addition, the fine powders prepared by low temperature calcination (about 400°C) probably retain a larger quantity of carbon contamination.

Increasing the rate of heating leads to the formation of closed pores before there is time for the carbon to react and escape and thus enhances the entrapment of CO and the formation of intergranular porosity.

Increasing the green density also leads to more rapid pore closure (see Fig. 6) since the density difference between samples of differing green density is essentially maintained at temperatures up to 1400–1500°C.

In addition the appearance of a peripheral zone of intragranular porosity probably results from the greater possibility of CO escape in the immediate vicinity of the surface. (But it may also be affected by contaminants from the furnace atmosphere).

5 Reproducibility

Finally, the influence of such a small amount of residual carbon and the competing processes of CO formation, escape, and pore closure during the period of rapid heating explain the difficulty that has been experienced in obtaining completely reproducible results between different lots of starting material, even when they apparently have identical physico-chemical charac-teristics (surface area, particle size, O/U ratio, etc. . .).

V CONCLUSIONS

1. Our results indicate that a very small carbon contamination (of the order of 10 ppm) present at a critical point during sintering when the porosity

becomes closed can have an important influence on the course of densification.

2. If CO formed by reaction of carbon with UO_2 is trapped in closed pores an appreciable pressure develops in the pores and there is localization of the residual porosity at grain junctions. The pore shape observed and the small dihedral angles found are believed to result from the presence of gas in the pores.

3. The small value of the dihedral angle (~90°) which results leads necessarily to stability of an 'intergranular' microstructure and a stopping of further shrinkage.

4. When using a rapid heating rate (100°C/minute) with a particle size and forming pressure favoring the development of intergranular porosity, sintering during heating is sufficiently rapid that the final density and type of microstructure are reached by the time the sample arrives at the sintering temperature of 1600–1700°C.

5. The interpretation given allows one to identify and evaluate those parameters favorable for the appearance of intergranular porosity. That is, the influence of increased surface area, increased green density, and increased heating rate can be rationally understood and controlled.

REFERENCES

1. B. Francois, R. Delmas, R. Caillat, P. Lacombe, *J. Nucl. Mat.*, **15**, 1, 105–110 (1965).
2. B. Francois, R. Delmas, R. Caillat, P. Lacombe, *C.R. Ac. Sc.*, **256**, 925–926 (1963).
3. M. Podest, L. Jakesova, Proceedings of the Conference on New Nuclear Materia'. Technology, including Non Metallic Fuel Elements, held by the I.A.E.A. at Prague, July 1963—I.A.E.A., Vienna (1963).
4. Y. Carteret, M. Portnoff, J. Elston, R. Caillat, Fourth International Symposium on the Reactivity of Solids, Amsterdam (1960), Elsevier Publishing Co, Amsterdam, 540–548 (1961).
5. W. D. Kingery, B. Francois, 'Grain Growth in Porous Compacts', *J. Am. Cer. Soc.*, **48**, 546–7 (1965).
6. C. H. Desh, *J. Inst. Metals*, **22**, 241 (1919).
7. F. C. Hull, W. J. Houk, *J. Metals*, **5**, 565 (1953).
8. C. S. Smith, Metal Interfaces, *Am. Soc. Metals*, p. 69 (1952).
9. W. D. Kingery, *J. Am. Cer. Soc.*, **37**, 42 (1954).
10. R. L. Coble, Private communication (1964).
11. W. D. Kingery, B. Francois, 'The Sintering of Crystalline Oxides—I—Interactions Between Grain Boundaries and Pores', *Sintering and Related Phenomena*, G. C. Kuczynski, W. Hooten and C. Gibson, Eds, Gordon & Breach, New York, 471–496 (1967).